

Coupling nonpolar and polar solvation free energies in implicit solvent models

J. D. Zubiella, J. M. J. Swanson, and J. A. McCammon

NSF Center for Theoretical Biological Physics (CTBP), and

Department of Chemistry and Biochemistry,

University of California, San Diego, La Jolla, California 92093-0365

(dated: December 23, 2021)

Abstract

Recent studies on the solvation of atomistic and nanoscale solutes indicate that a strong coupling exists between the hydrophobic, dispersion, and electrostatic contributions to the solvation free energy, a facet not considered in current implicit solvent models. We suggest a theoretical formalism which accounts for coupling by minimizing the Gibbs free energy of the solvent with respect to a solvent volume exclusion function. The resulting differential equation is similar to the Laplace-Young equation for the geometrical description of capillary interfaces, but is extended to microscopic scales by explicitly considering curvature corrections as well as dispersion and electrostatic contributions. Unlike existing implicit solvent approaches, the solvent accessible surface is an output of our model. The presented formalism is illustrated on spherically or cylindrically symmetrical systems of neutral or charged solutes on different length scales. The results are in agreement with computer simulations and, most importantly, demonstrate that our method captures the strong sensitivity of solvent expulsion and dewetting to the particular form of the solvent-solute interactions.

I. INTRODUCTION

Implicit solvent models are widely used in theoretical chemistry to study the solvation of biomolecular systems, as well described in the review of Roux and Simonson¹. They provide a more efficient, although generally less accurate, alternative to atomistically-resolved explicit solvent simulations. The solvation free energy in these models is usually split into nonpolar (np) and polar (p) terms,

$$G = G_{np} + G_p; \quad (1)$$

which are treated in separate energetic evaluations. The nonpolar term includes the energetic cost of cavity formation, solvent rearrangement, and solute-solvent dispersion interactions introduced when the uncharged solute is brought from vacuum into the solvent environment. The polar term describes the free energy of charging the mono- or multipolar solute in the dielectric medium.

The nonpolar term is commonly approximated by surface area models, i.e. $G_{np} \propto S$, where S is the solvent accessible surface area² and γ is an energy per surface area constant, which is a priori not known but fit to atomistic simulations. The deficiencies of this simple surface area approach have been recognized and a further decomposition of the nonpolar term into cavity (cav) and van der Waals dispersion (vdW) terms has been proposed,^{3,4}

$G_{np} = G_{cav} + G_{vdW}$. This approach has shown improved results for the solvation of alkanes,^{3,5} the alanine peptide,⁶ and nonpolar native and misfolded proteins.⁷ The electrostatic (polar) contribution of the solvation free energy is often approximated by generalized Born⁸ (GB) or Poisson-Boltzmann⁹ (PB) models. Both methods use a position-dependent dielectric constant,¹ assigned on the basis of the solute surface, which can be defined in several ways,¹⁰ or defined implicitly by integration methods. It has been emphasized that all three contributions, G_{cav} , G_{vdW} , and G_p depend critically on the location of the solvent-solute interface. It has also been shown that the effective location of the solvent-solute interface can vary according to the local electrostatic¹¹ and dispersion¹² potentials. This suggests that interfacial, dispersion and electrostatic contributions should be coupled in implicit solvent approaches. The importance of capturing the right balance between nonpolar and electrostatic contributions in implicit solvation models was emphasized by Ashbaugh et al. in their study of amphiphiles.¹³

The significance of nonpolar and polar coupling becomes even more evident when solvation is studied on length scales which are large compared to the solvent molecule (typically ~ 1 nm for water), where solvent dewetting ("drying") can occur. In this mechanism, first envisioned by Stillinger,¹⁴ the solvent molecules tend to move away from the surface of a large nonpolar solute forming a liquid-gas like interface parallel to the solute interface. When the surfaces of two large solutes come together dewetting can be amplified due to the gain of interfacial free energy (by decreasing the total liquid-vapor interface area) giving rise to a strong effective attraction.^{15,16,17} Early evidence of confinement-induced dewetting was given only by explicit water simulations for smooth plate-like solutes with a purely repulsive solute-solvent interaction.¹⁸ More recently, however, it has been demonstrated in varying degrees in several systems with attractive solute-solvent interactions including smooth parallel plate-like solutes,¹⁹ atomistically resolved paraffin-plates,²⁰ graphite-plates²¹, carbon nanotubes,²² and hydrophobic ion channels.^{23,24,25}

Several of these studies indicated that the magnitude of dewetting is sensitive to the nature of the solute-solvent attractive dispersion interactions.^{19,20,21} A similar sensitivity was found in systems where the solutes carry charges or are exposed to an external electric field, e.g. electrostatic interactions have been shown to strongly affect the dewetting behavior of hydrophobic channels^{26,27,28} and hydrophobic spherical nanosolutes.^{29,30} Furthermore, two recent simulations of proteins supported the importance of solvent dewetting and its sensitivity in realistic biomolecular systems. First, a simulation of the two-domain BphC enzyme showed that the region between the two domains was completely dewetted when vdW and electrostatic interactions were turned off, but accommodated 30% of the bulk density with the addition of vdW attraction (water was found mainly at the edges of the considered volume, while the central region was still empty), and 85-90% with the addition of electrostatic interactions.³¹ Second, Liu et al. observed a clear dewetting transition in the simulation of the collapse of the melittin tetramer, which was strongly sensitive to the type and location of the hydrophobic residues around the dewetted region.³²

Considering the aforementioned studies, we postulate that coupling of the nonpolar and polar solvation contributions in implicit solvent models is crucial for an accurate determination of solvation free energies without too many system-dependent fit parameters. We suggest a general theoretical formalism in which the particular energetic contributions are coupled. Similar to the approach of Parker et al. in their study of bubble formation at hy-

drophobic surfaces,³³ we express the Gibbs free energy as a functional of the solvent volume exclusion function,³⁴ and obtain the optimal solute surface via minimization. As we will show, this minimization leads to an expression which is similar to the Laplace-Young equation for the description of macroscopic capillary interfaces,³⁵ but is generalized to explicitly include curvature corrections and solvent-solute interactions, i.e. short-range repulsion (excluded volume), dispersion, and electrostatics. This extension of the Laplace-Young theory allows a geometric description of solvation on mesoscopic and microscopic scales. Related approaches in other fields are the Helfrich description of vesicle and membrane surfaces,^{36,37} wetting in colloids and granular media,^{35,38} and functional treatments of electrowetting.³⁹

While most implicit solvent approaches define the solute surface with a geometric evaluation of the molecular surface, vdW surface, or canonical solvent accessible surface (SAS),^{2,10} it is an output of our theory. The surface obtained by minimizing our free energy functional will, in general, be very different than the aforementioned established surface definitions. In particular, our solvent accessible surface should not be confused with the canonical SAS,² which is simply the envelope surrounding probe-inflated spheres. Similarly, phenomenological continuum theories applied to solvent dewetting always assume a certain, simplified geometry for the dry region, e.g. a cylindrical volume for system like hydrophobic ion channels,^{24,28,40} plate-like particles,^{15,19} or two hydrophobic spherical solutes.⁴¹ For a few simple systems this might be a valid approximation but for more complicated solute geometries the shape of the dewetted volume is unknown and a different approach, as suggested in this work, is necessary. We expect our formalism to be particularly useful in solvation studies of large protein assemblies where the hydrophobic surfaces are highly irregular and laced with hydrophilic units,^{42,43} and for which a unified description of hydration on different length scales is important.¹⁷ Another potential application is the solvation of superhydrophobic nanosolutes⁴⁴ and wetting/dewetting in near-critical colloidal mixtures.³⁸

A brief summary of our work has been published elsewhere.⁴⁵ Here we present more challenging test cases and an expanded discussion of the approximations and limitations of this model. The rest of the paper is organized as follows: In section II we present our theoretical formalism and chosen approximations. In section III we first verify that our method can describe solvation on molecular scales with noble gases, ions, and small alkanes. We then demonstrate that it captures the strong sensitivity of dewetting and hydrophobic hydration to specific solute-solvent interactions on larger scales with two alkane-assembled

spheres. In section IV we conclude with some final remarks.

II. THEORY

A. Basic formalism

Let us consider an assembly of solutes with arbitrary shape and composition surrounded by a dielectric solvent in a volume W . Furthermore, we define a subvolume (or cavity) V empty of solvent for which we can assign a volume exclusion function given by

$$v(\mathbf{r}) = \begin{cases} 0 & \text{for } \mathbf{r} \in V; \\ 1 & \text{else;} \end{cases} \quad (2)$$

We assume that the surface surrounding the volume is continuous and closed, i.e. has no boundary. The absolute volume V and surface area S of V can then be expressed as functionals of $v(\mathbf{r})$ via

$$\begin{aligned} V[v] &= \int_V d^3r [1 - v(\mathbf{r})] \\ S[v] &= \int_W d^3r |\nabla v(\mathbf{r})| \end{aligned} \quad (3)$$

where $\nabla = \nabla_{\mathbf{r}}$ is the usual gradient operator with respect to the position vector \mathbf{r} and $|\nabla v(\mathbf{r})|$ gives a δ -function-like contribution only at the volume boundary. The expression $\int_W d^3r |\nabla v(\mathbf{r})| = \int dS$ can thus be identified as the infinitesimal surface element. In this continuum solvent model the solvent density distribution is simply $\rho(\mathbf{r}) = \rho_0 v(\mathbf{r})$, where ρ_0 is the bulk density of the solvent at the desired temperature and pressure. Local inhomogeneities of the solvent density, apart from the zero to ρ_0 transition at the volume boundaries, are neglected. The solutes' positions and conformations are fixed such that the solutes can be considered as an external potential to the solvent without any degrees of freedom.

As motivated before, we suggest expressing the Gibbs free energy $G[v]$ as a functional of the volume exclusion function $v(\mathbf{r})$, and obtaining the optimal solute volume via minimization

$$\delta G[v] / \delta v(\mathbf{r}) = 0; \quad (4)$$

where $\delta/\delta v$ denotes the functional derivative with respect to the function v . We adopt following ansatz for the Gibbs free energy of the solvent:

$$\begin{aligned} G[v] &= G_{pr}[v] + G_{int}[v] + G_{ne}[v] + G_{es}[v] \\ &= P V[v] + \int_V d^3r \gamma(\mathbf{r}; [v]) \delta v(\mathbf{r}) \\ &\quad + \int_V d^3r v(\mathbf{r}) U(\mathbf{r}) \\ &\quad + \int_V d^3r \frac{\epsilon_0}{2} (\mathbf{r}; [v]) [\mathbf{E}(\mathbf{r})]^2 + v(\mathbf{r}) U_{mi}(\mathbf{r}) \end{aligned} \quad (5)$$

Let us discuss each of the terms in Eq. (5) in turn. The first term, $G_{pr}[v]$, proportional to the volume V , is the energy of creating a cavity in the solvent against the difference in bulk pressure between the liquid and vapor phase, $P = P_l - P_v$. For water in ambient conditions, which is close to the liquid-vapor transition, this term is relatively small and can generally be neglected for solutes on molecular scales. The second term $G_{int}[v]$ describes the energetic cost due to solvent rearrangement around the cavity interface with area S in terms of a free energy/surface area functional $\gamma(\mathbf{r}; [v])$. This interfacial energy penalty is thought to be the main driving force behind hydrophobic phenomena.¹⁷ γ is a solvent specific quantity that also depends on the particular topology of the cavity-solvent interface, i.e. it varies locally in space and is a functional of the volume exclusion function $\gamma = \gamma(\mathbf{r}; [v])$.⁴⁶ The exact form of this functional is not known.

The third term, $G_{ne}[v]$, is the total energy of the non-electrostatic solute-solvent interaction given a solvent density distribution $\rho_0 v(\mathbf{r})$. The potential $U(\mathbf{r}) = \sum_i U_i(\mathbf{r} - \mathbf{r}_i)$ is the sum of the (short-ranged) repulsive exclusion and (long-ranged) attractive dispersion interaction between each solute atom i at position \mathbf{r}_i and a solvent molecule at \mathbf{r} . Classical solvation studies typically represent the interaction U_i as an isotropic Lennard-Jones (LJ) potential,

$$U_{LJ}(r) = 4 \left[\frac{\epsilon}{r^{12}} - \frac{\epsilon}{r^6} \right]; \quad (6)$$

with an energy scale ϵ , length scale σ , and center-to-center distance r . Using the form of (6) implies that $v(\mathbf{r})$ is defined with respect to the LJ-centers of the solvent molecules.

The last term, $G_{es}[v]$, describes the total energy of the electrostatic field and the mobile ions in the system expressed by the local electrostatic potential $\phi(\mathbf{r})$ assuming linear response of the dielectric solvent.⁴⁷ Similar to $\gamma(\mathbf{r}; [v])$, the position-dependent dielectric constant

$\psi(\mathbf{r}) = \psi(\mathbf{r}; [v])$ depends on the geometry of $v(\mathbf{r})$ with an unknown functional form. $\rho(\mathbf{r})$ is the fixed charge density distribution of the solutes and the local energy density of the mobile ions is^{9,48}

$$U_{mi}(\mathbf{r}) = k_B T \sum_j^X c_j \exp[-q_j \psi(\mathbf{r})] \quad (7)$$

with the thermal energy $k_B T = 1$. Variation of (5) for a fixed $v(\mathbf{r})$ with respect to $\psi(\mathbf{r})$ yields the Poisson-Boltzmann equation^{9,48}

$$\begin{aligned} \text{PB}(\mathbf{r}) = 0 = -\nabla^2 \psi(\mathbf{r}; [v]) + \rho(\mathbf{r}) \\ + v(\mathbf{r}) \sum_j^X q_j c_j \exp[-q_j \psi(\mathbf{r})]; \end{aligned} \quad (8)$$

where q_j and c_j are the charge and concentration of the mobile ion species j . Note that the ionic charge density in (8) is multiplied by $v(\mathbf{r})$ to account for the fact that ions usually cannot penetrate the volume empty of polar solvent due to a huge free energy penalty. We remark that the treatment of the electrostatics in our theory has the same limitations as other implicit models using PB, for instance when describing highly charged or strongly correlated electrolyte systems. In contrast to PB/SA models however, the dielectric boundary is optimized such that it responds to the local nonpolar and polar potential; it is not assumed beforehand.

Let $v_{min}(\mathbf{r})$ be the exclusion function which minimizes the functional (5). Then, the resulting Gibbs free energy of the system is given by $G[v_{min}]$. The solvation free energy G is the reversible work to solvate the solute and is given by

$$G = G[v_{min}] - G_0; \quad (9)$$

where G_0 is a constant reference energy which can refer to the pure solvent state and an unsolvated solute. The potential of mean force (pmf) along a given reaction coordinate x (e.g. the distance between two solutes' centers of mass) is given, within a constant, by $G[v_{min}]$, where $v_{min}(\mathbf{r})$ must be evaluated for every x . In order to proceed we will need valid approximations for $\psi(\mathbf{r}; [v])$ and $\rho(\mathbf{r}; [v])$ with which $v_{min}(\mathbf{r})$ can be calculated by explicitly minimizing our free energy functional (5) according to (4).

B. Approximations for $\gamma(\mathbf{r}; [v])$ and $\gamma(\mathbf{r}; [v])$

Let us start with a possible description of $\gamma(\mathbf{r}; [v])$. For a planar macroscopic interface the parameter γ is usually identified by the surface tension of the solvent adjacent to the second medium. This surface tension obviously depends on the microscopic interactions between the medium and the solvent and is generally decreased by attractive dispersion or electrostatic contributions. It seems that microscopic interactions are adequately represented by a macroscopic quantity like γ if their range is much smaller than the investigated length scales, such as the radii of curvature or mean particle distances. The effect of the microscopic interactions are then absorbed in γ . This has been exemplified with free energy estimates for the solvation of large, neutral plate-like or spherical alkane-assembled solutes,^{12,19} For the description of solvation on smaller length scales, however, it seems important to separate the free energy into a part which accounts for the formation of a cavity and a part which describes the dispersion interactions explicitly.³ Furthermore, it has been shown that the water liquid-vapor surface tension γ_{lv} is the asymptotic value of the solvation free energy per surface area for hard spherical cavities in water in the limit of large radii.^{15,49} These considerations motivate our choice of the second and third term in the functional (5) and lead to the assumption γ_{lv} in the limit of vanishing curvatures.

The surfaces of realistic (bio)molecules, however, display highly curved shapes, so $\gamma(\mathbf{r}; [v])$ will strongly depend on the interface geometry around \mathbf{r} in a complicated fashion. In the following we make a local curvature approximation, i.e. we assume that $\gamma(\mathbf{r}; [v])$ can be expressed solely as a function of the local mean curvature

$$H(\mathbf{r}) = (\kappa_1(\mathbf{r}) + \kappa_2(\mathbf{r}))/2 = R(\mathbf{r})^{-1}; \quad (10)$$

where $R(\mathbf{r})$ is the radius of mean curvature and $\kappa_1(\mathbf{r})$ and $\kappa_2(\mathbf{r})$ are the local principal curvatures of the interface.⁵⁰ The mean curvature H is only defined at the boundary of $v(\mathbf{r})$. We have chosen the convention in which the curvatures are positive for convex surfaces (e.g. a spherical cavity) and negative for concave surfaces (e.g. a spherical droplet).

The curvature dependence of the liquid-vapor surface tension has been a long standing subject of research and is still under steady discussion.^{38,51,52} For water, which is close to the critical point under ambient conditions, γ is argued to be nonanalytical in curvature.⁵² The first order correction term, however, is likely to be linear in curvature as predicted by scaled-particle theory,⁵³ the commonly used ansatz to study the solvation of hard spherical

cavities. Although this result is only strictly valid for the case of spherical particles, we assume that it can be applied to local mean curvatures such that $\gamma(\mathbf{r}; [v])$ reduces to the function

$$\gamma(\mathbf{r}) = \gamma_{lv} (1 - \frac{1}{2} H(\mathbf{r}) \ell); \quad (11)$$

where ℓ is the Tolman length, which is expected to be of molecular size.⁵⁴ In our study we assume γ_{lv} is constant and positive, while the curvature can be positive or negative as defined above. Note that this leads to an increase of surface tension for concave surfaces in agreement with the geometrical arguments of Honig et al.⁵⁵ in their solvation study of alkanes. It has been shown by computer simulations of growing a hard spherical cavity in water that (11) predicts the interfacial energy rather well for radii $\geq 3\text{\AA}$.⁴⁹ A major drawback of approximation (11) is that it gives unphysical results if the radius of mean curvature is smaller than twice the Tolman length, $|R| < 2\ell$. It yields negative and diverging surface tensions for convex and concave surfaces, respectively. The latter is not possible due to the finite size of the solvent molecules. Thus, care has to be taken with approximation (11) when investigating systems which can exhibit radii of curvature $|R| < 2\ell$.

Let us now turn to electrostatics. The most common approximation for the position-dependent dielectric constant is proportional to the volume exclusion function $v(\mathbf{r})$,¹ such that the functional $\gamma(\mathbf{r}; [v])$ reduces to,

$$\gamma(\mathbf{r}) = \gamma_v + v(\mathbf{r}) (\gamma_1 - \gamma_v); \quad (12)$$

where γ_v and γ_1 are the dielectric constants inside and outside the volume V , respectively. Eq. (12) is valid only in the limit of large solute sizes when the molecular size of the solvent is negligible. For charged solutes on a molecular scale, let's say mono- or polyvalent ions, two difficulties arise. First the electric field close to the highly curved solutes can be strong enough for the dielectric constant to be field dependent. This formally affects the form of the electrostatic term in the free energy functional which assumes a linear response of the solvent. An improvement for continuum models along these lines has been proposed by Luo et al.⁵⁶ Second, the effective position of the dielectric boundary is known to depend on the sign of the solute charge for asymmetric solvent molecules like water. This expresses itself, for instance, in different Born radii for two equally charged ions which have exact the same LJ parameters but a different sign of charge. A reasonable improvement of (12) would be to

shift the dielectric boundary at \mathbf{r} parallel to the volume boundary by a potential dependent amount $\delta\mathbf{r} = -(\epsilon(\mathbf{r})/\epsilon_1)\mathbf{n}(\mathbf{r})$:

$$\epsilon(\mathbf{r}) = \epsilon_v + \epsilon(\mathbf{r} - \delta\mathbf{r}) (\epsilon_1 - \epsilon_v); \quad (13)$$

where \mathbf{n} is the unit normal vector to the interface. We do not attempt however, to find an approximation for the function $\epsilon(\mathbf{r})$ in this work and postpone this investigation to later studies. For further illustration of our approach we content ourselves with the approximations (11) for $\epsilon(\mathbf{r}; [v])$ and (12) for $\epsilon(\mathbf{r}; [v])$.

C. Minimization of the free energy functional

For the functional derivative of the interfacial term, $G_{\text{int}}[v]$, we utilize

$$\frac{\delta}{\delta v} \int_{V_W} d^3r \nabla \cdot \mathbf{v}(\mathbf{r}) = \frac{\delta}{\delta v} \int_{\partial W} dS = 2H \quad (14)$$

and

$$\frac{\delta}{\delta v} \int_{V_W} d^3r H \nabla \cdot \mathbf{v}(\mathbf{r}) = \frac{\delta}{\delta v} \int_{\partial W} dS H = K; \quad (15)$$

which has been derived in detail by Zhong-can and Helfrich by means of differential geometry.³⁶ The variable $K(\mathbf{r}) = \epsilon_1(\mathbf{r}) - \epsilon_2(\mathbf{r})$ is the Gaussian curvature of the interface, which is an intrinsic geometric property of v . Plugging in approximations (11) and (12) into (5), and minimizing with (4), we obtain,

$$0 = \delta \epsilon(\mathbf{r}) = P + 2 \int_{V_W} [H(\mathbf{r}) - K(\mathbf{r})] \epsilon_0 U(\mathbf{r}) \\ - \frac{\epsilon_0}{2} [\epsilon(\mathbf{r}) - \epsilon_1]^2 - \frac{1}{\epsilon_1} - \frac{1}{\epsilon_v} U_{\text{mi}}(\mathbf{r}); \quad (16)$$

Eq. (16) is a partial second order differential equation ($\delta \epsilon$) for the optimal exclusion function $v_{\text{min}}(\mathbf{r})$ expressed in terms of pressure, curvatures, short-range repulsion, dispersion, and electrostatic terms, all of which have dimensions of energy density. It can also be interpreted as a mechanical balance between the forces per surface area generated by each of the particular contributions. Thus, in our approach the surface shape and geometry, expressed by H and K , are directly related to the inhomogeneous potential contributions. The constant solute charge density $\epsilon(\mathbf{r})$ does not appear explicitly in (16) but is implicitly considered in

the PB equation (8), which must be solved simultaneously. If curvature correction (K -term) and the last three energetic terms are neglected one obtains the Laplace-Young equation,

$$P = -2\gamma H; \quad (17)$$

which is exclusively used for the shape description of macroscopic capillary and interfacial phenomena in conjunction with appropriate boundary conditions, e.g. prescribed liquid-solid contact angles at the solid surfaces.³⁵ In our description the boundary conditions are provided by the constraints given by the short-ranged repulsive term in $U(\mathbf{r})$, and the distribution of dispersion and electrostatics, allowing an extrapolation of the Laplace-Young description to mesoscopic and microscopic scales. Notice that in our approach the solvent is treated as a continuum while the solute is explicitly resolved. One could use a coarse-grained treatment for the solute by including the appropriate non-electrostatic and electrostatic interactions in (5).

The solution of (16) requires an appropriate parametrization, i.e. coordinate representation, for the curvatures H and K , such that the equation is expressed as a function of the vector \mathbf{r} and its first and second derivatives in space. Analytical solutions to the much simpler Eq. (17) and thus to (16) are only available for systems with very simple geometries.³⁵ Thus we use numerical solutions of (16) in the following to further illustrate our theory.

III. APPLICATIONS

First, we will consider the solvation of microscopic solutes such as noble gases, simple alkanes, and ions which can be treated as neutral or charged Lennard-Jones spheres. Then, we will investigate alkane assemblies on a larger scale where interfacial and wetting effects are much more dominant. For simplicity and a better transparency of the results, mobile ions will be neglected in these illustrations.

A. One Lennard-Jones sphere

In this section we compare our approach to results from SPC and SPC/E explicit solvent simulations.⁵⁷ We refrain from comparing to real experiments since approximations in computer experiments are more easily controlled and the LJ parameters of the solutes are commonly parametrized to yield accurate results in classical simulations.

For a spherical solute with a charge Q homogeneously distributed over its surface, the functional (5) with approximations (11) and (12) and no mobile ions reduces to a function of R , the radius of the sphere empty of solvent. The solvation free energy is

$$\begin{aligned}
 G(R) &= G_{pr}(R) + G_{int}(R) + G_{ne}(R) + G_{es}(R) \\
 &= \frac{4}{3} R^3 P + 4 R^2 \gamma_{lv} - \frac{2}{R} \\
 &\quad + \int_0^R 4 r^2 dr \epsilon_0 U_{LJ}(r) \\
 &\quad + \frac{Q^2}{8 \epsilon_0 R} \left(\frac{1}{\epsilon_1} - \frac{1}{\epsilon_v} \right) ;
 \end{aligned} \tag{18}$$

Note that the last term in (18) is equivalent to the Born electrostatic solvation free energy.¹ Recently, Manjari et al. have presented a very similar expression for the solvation of a charged spherical cavity on the basis of a minimization principle and have investigated the variation of R with thermodynamic conditions.⁵⁸ Differentiation of (18) with respect to R and subsequent division by $4 R^2$ yields

$$\begin{aligned}
 0 &= P + \frac{2 \gamma_{lv}}{R} - \frac{1}{R^2} - \epsilon_0 U_{LJ}(R) \\
 &\quad - \frac{Q^2}{32 \pi \epsilon_0 R^4} \left(\frac{1}{\epsilon_1} - \frac{1}{\epsilon_v} \right) ;
 \end{aligned} \tag{19}$$

which is in accord with Eq. (16) given sphere-like curvatures, $H = 1/R$ and $K = 1/R^2$. We can now calculate the solvation free energies of simple spherical solutes, such as noble gases or ions. The free parameters in Eq. (19) are the pressure P , Tolman length δ , liquid-vapor surface tension γ_{lv} , and dielectric constants ϵ_v and ϵ_1 .

1. One neutral LJ sphere

First, let us focus on uncharged spheres, for which the electrostatic term in (18) can be neglected. We compare the results from our theory to those calculated by Hummer et al.⁵⁹ for neutral LJ spheres in SPC water, and those calculated by Paschek⁶⁰ for noble gases in SPC and SPC/E water. The solute-water LJ parameters and δ are summarized in Tab. I. The surface tension γ_{lv} was set to that estimated for SPC and SPC/E water at 300K, $\gamma_{lv} = 65 \text{ mJ/m}^2$ and $\gamma_{lv} = 72 \text{ mJ/m}^2$, respectively.^{49,61} The pressure is fixed to 1 atm. Finally, the remaining free parameter was fit to reproduce the simulation solvation free

energies exactly. The solvation free energies from simulation G_{sim} and best fit Tolman lengths b_{f} are shown in Tables I and II for the SPC and SPC/E models, respectively.

Before we discuss the results, let us compare the particular energy contributions $G_i(R)$ with $i = \text{pr}, \text{int}, \text{ne}$ for Na^0 (plotted in Fig. 1). As anticipated, the pressure term $G_{\text{pr}}(R)$ with $P = 1 \text{ atm}$ is negligible compared to the other contributions. The interfacial term $G_{\text{int}}(R)$ increases with the cavity radius R . The integrated LJ-interaction term $G_{\text{ne}}(R)$ shows long-range attraction and a steep short-ranged repulsion with a minimum at $R = (N a^0) = 2.85 \text{ \AA}$. The total solvation free energy for the Na^0 shows a single minimum at $R_{\text{min}} = 2.32 \text{ \AA}$ with $G = -9.2 \text{ kJ/mol}$ for a $b_{\text{f}} = 0.79 \text{ \AA}$.

The results for the other LJ-spheres, summarized in Tab. I and II, reveal several noteworthy observations. First, the best fit Tolman lengths b_{f} range from 0.76 \AA to 1.00 \AA ; they are not only of molecular size, as expected, but are approximately half the LJ-radius of a SPC or SPC/E water molecule. Second, the b_{f} values for noble gases in SPC/E water (Tab. II) are approximately 10% larger than those in SPC water (Tab. I). This is in qualitative agreement with the results of Huang et al. who measured $b_{\text{f}} = 0.76 - 0.9 \text{ \AA}$ and $b_{\text{f}} = 0.90 - 1.0 \text{ \AA}$ for SPC and SPC/E, respectively, by fitting Eq. (11) to the hydration free energy of hard spheres with varying radii.⁴⁹

Third, the quite accurate data of Paschek demonstrate a systematic increase of b_{f} with solute size. The inability of our theory to be fitted by one fixed constant b_{f} points to the anticipated fact that Eq. (11) can not capture strong curvature effects accurately and will have to be refined for small solutes. Despite this shortcoming, these results show surprisingly good agreement; if we assume a fixed delta, for instance $b_{\text{f}} = 0.9 \text{ \AA}$ for all noble gases in the SPC data of Paschek, our theory predicts results within 15% of the simulation data. Finally, we observe that the effective optimal sphere radius R_{min} is always smaller than the radius of the canonical SAS with a typical probe radius of 1.4 \AA ,⁶² $R_{\text{min}} < (r_{\text{ss}} = 2 + 1.4 \text{ \AA})'$, but larger than the vdW surface, $R_{\text{min}} > r_{\text{ss}} = 2$, where r_{ss} is the solute-solute LJ-length.⁶³

2. One charged LJ sphere

Let us now turn to charged Lennard-Jones spheres (ions) also examined in the paper by Hummer et al. with SPC water simulations. We assume b_{f} to be fixed by the previously obtained b_{f} values for uncharged spheres. The dielectric constants are set to $\epsilon_v = 1$ and $\epsilon_l =$

65, in accord with SPC water.⁶⁴ The electrostatic contribution $G_{es}(R)$ and the total $G(R)$ for Na^+ are shown in the inset of Fig. 1. The electrostatic contribution decreases the optimal radius to $R_{min} = 1.83\text{\AA}$ giving a solvation free energy of $G = -334\text{kJ/mol}$. In fact, the optimal sphere radius R_{min} is always considerably smaller for the charged solutes (Tab. III) than for their neutral counterparts (Tab. I). This is caused by the strong compressing force of the polar solvent attempting to penetrate the low dielectric cavity. The solvation free energies from theory G and those from simulation G_{sim} are also shown in Tab. III. While our theory describes the hydration free energies for positively charged ions within 15%, it considerably underestimates those of the negative ions. This qualitative disagreement between positive and negative ions was expected since the Born radii for anions are always smaller than those for cations, a consequence of the different solvation structure around charged solutes with opposite signs. As mentioned in the previous section, the position of the dielectric boundary has to be refined for accurate estimates of the electrostatic contribution to the hydration free energy. If we apply the correction (13) to the dielectric boundary with a simple, potential-independent shift $\delta_+ = 0.25\text{\AA}$ for positive and $\delta_- = 1.05\text{\AA}$ for negative spheres such that the dielectric boundary has a radius of $R + \delta < R$, improved values (G in Tab. III) are obtained which reproduce all simulation values within 10%!

B. Linear alkanes

Let us now consider simple polyatomic molecules, such as ethane, propane, or butane in a cylindrically symmetric one-dimensional (1D) chain conformation. Other conformations will be neglected. The symmetry of these systems allows us to express the volume exclusion function $v(r)$ of the enveloping surface by a one dimensional shape function $r(z)$, where z is the coordinate on the symmetry axis and r the radial distance to it. The full surface in three-dimensional space is obtained by revolving the shape function $r(z)$ around the symmetry axis. Technical details are given in the Appendix.

The LJ parameters for ethane and methane are the same as those used by Ashbaugh et al.¹³ in their SPC simulation of linear alkanes (see Tab. I). The simulation solvation energy of the spherical methane, $G = -10.96\text{kJ/mol}$, can be reproduced with $\delta_{bf} = 0.85\text{\AA}$. Solving the cylindrically symmetric problem for ethane using the same δ , we obtain a δ -parameter free $G = -11.40\text{kJ/mol}$, which is only 7% larger than the simulation results. Alternatively,

$r_{bf} = 0.87\text{\AA}$ reproduces the simulation energy exactly. This is surprisingly good agreement considering the crudeness of our curvature correction and the fact that the large curvature of the system varies locally in space. The curvature and shape functions are plotted in Fig. 2 together with the vdW surface and the canonical SAS obtained from rolling a probe sphere with the typically chosen radius $r_p = 1.4\text{\AA}$ over the vdW surface.⁶² Away from the center of mass $|z| \gg 1\text{\AA}$ the curvatures follow the expected trends for the spherical surfaces: $H = 1/R$ and $K = 1/R^2$ with $R \gg 3.1\text{\AA}$. The optimal surface resulting from our theory is smaller than the canonical SAS and smooth at the center of mass ($z = 0$) where the canonical SAS has a kink. Thus our surface has a smaller mean curvature at $z = 0$ and an almost zero Gaussian curvature, which is typical for a cylinder geometry with one principal curvature equal to zero. These results may justify the use of smooth surfaces in coarse-grained models of closely-packed hydrocarbons, a possibility we will explore in the following section with solvation on larger length scales where dewetting effects can occur. If we repeat the above calculation for propane and butane (three and four LJ-spheres, see also Tab. I for parameters) we need $r_{bf} = 0.94\text{\AA}$ and $r_{bf} = 0.96\text{\AA}$, respectively, to reproduce the simulation results exactly. The increasing difference in r_{bf} compared to methane and ethane is likely due to contributions from other than cylindrically symmetric conformations which were ignored in our analysis.

C. Two spherical nanosolutes

1. Model

Let us now consider two spherical solutes which represent homogeneously assembled CH_2 groups with a uniform density $\rho = 0.024\text{\AA}^{-3}$ up to a radius $R_0 = 15\text{\AA}$, defined by the maximal distance between a CH_2 center and the center of the solute. Integration of the CH_2 -water LJ interaction over the entire sphere yields a 9-3 like potential $U_i(r)$ for the interaction between the center of the solute ($i = 1, 2$) and a water molecule.¹² The intrinsic, nonelectrostatic solute-solute interaction U_{ss} can be obtained in a similar fashion. The CH_2 -water LJ parameters, $\epsilon = 0.5665\text{kJ/mol}$ and $\sigma = 3.52\text{\AA}$, are taken from the OPLSUA force-field⁶⁵ and are similar to those used by Huang et al. in their study on dewetting between parallel plates.²⁰ Minimizing Eq. (18) for just one sphere we obtain an optimal solvent excluded

radius of $R_{\text{min}} = 17.4\text{\AA}$, which is $R_0 + 2.4\text{\AA}$. Since we are also interested in the effects of electrostatic interactions we place opposite charges $\pm Ze$, where e is the elementary charge, in the center or on the edge of the two spheres. Poisson's equation is simultaneously solved on a two-dimensional grid in cylindrical coordinates. Numerical details are given in the Appendix.

The solvation of the two solutes is studied for a fixed surface-to-surface distance which we define as $s_0 = r_{12} - 2R_0$, where r_{12} is the solute center-to-center distance. The effective surface-to-surface distance defined by the accessibility of the solvent centers is thus $s = r_{12} - 2R_{\text{min}} = s_0 - 4.8\text{\AA}$. In the following we focus on a separation distance of $s_0 = 8\text{\AA}$ to investigate the influence of different energetic contributions on the shape function, $r(z)$, and the curvatures, $K(z)$ and $H(z)$. For $s_0 = 8\text{\AA}$, it follows that $s = 3.2\text{\AA}$, such that two water molecules could fit between the solutes on the z -axis. We systematically change the solute-solute and solute-solvent interactions, as summarized in Tab. I. We begin with only the repulsive part of the nonelectrostatic interaction $U_i(r)$ in system I, and then add a curvature correction with $\kappa = 0.75\text{\AA}$, vdW attractions, and sphere-centered charges $Z = 4$ and $Z = 5$ in systems II-V, respectively. To study the influence of charge location, we reduce the magnitude of each charge in system VI to $Z = 1$ and move them to the edge of the spheres on the symmetry axis such that they are 8\AA apart (indicated by arrows in Fig. 3. The surface tension and dielectric constants of the vapor (solute) and liquid are fixed to $\gamma_v = 72\text{mJ/m}^2$, $\epsilon_v = 1$, and $\epsilon_l = 78$, respectively.

2. Behavior of the shape function

The results for the curvatures and shape function, defined by $r(z)$, for systems I-VI are shown in Fig. 3. Away from the center of mass ($|z| \geq 10\text{\AA}$), systems I-VI show very little difference. The curvatures are $H = 1/R$ and $K = 1/R^2$ with $R = 17.4\text{\AA}$. Close to the center of mass ($z = 0$), however, the influence of changing the parameters is considerable. In system I, Eq. (16) reduces to the minimum surface equation $H(z) = 0$ for $z = 0$. For two adjacent spheres the solution of this equation is the catenoid $r(z) = \cosh(z)$, which features zero mean curvature (κ_1 and κ_2 cancel each other) and negative Gaussian curvature. As a consequence, the system exhibits a vapor bubble bridging the solutes, i.e. water is removed from the region between the spheres even though it fits there. This dewetting is driven by

the interfacial term G_{int} which always favors minimizing the liquid-vapor interface.

When curvature correction is applied (system II), the mean curvature becomes nonzero and negative (concave) at $z' = 0$, while the Gaussian curvature grows slightly more negative. Thus the total enveloping surface area becomes larger and the solvent inaccessible volume shrinks, i.e. the value of the shape function at $z' = 0$ decreases. Turning on solute-solvent dispersion attraction amplifies this trend significantly as demonstrated by system III. Mean and Gaussian curvatures increase severalfold, showing strongly enhanced concavity, and the volume empty of water decreases considerably, expressed by $r(z = 0) \approx 10.7A$ dropping to $r(z = 0) \approx 6.3A$. These trends continue with the addition of electrostatics in system IV. When the sphere charges are further increased from $Z = 4$ to $Z = 5$ (system IV \rightarrow V), we observe a wetting transition: the bubble ruptures and the shape function jumps to the solution for two isolated solutes, where $r(z' = 0) = 0$. The same holds when going from III to VI, when only one charge unit, $Z = 1$, is placed at each of the solutes' surfaces. Importantly, this demonstrates that the present formalism captures the sensitivity of dewetting phenomena to specific solvent-solute interactions as reported in previous studies.^{20,21,26,27,29,31,32} Note that the optimal shape function at $z' = 2A$ is closer to the solutes in VI compared to V due to the proximity of the charge to the interface. Clearly, the observed effects, particularly the transition from III to VI, cannot be described by existing solvation models which use the surface area (GB/SA or PB/SA)¹ or effective surface tensions and macroscopic solvent-solute contact angles^{33,35} as input.

3. Potential of mean force

The significant change of the shape function with the solute-solvent interaction has a strong impact on the potential of mean force (pmf) (or effective interaction) between the solutes

$$W(s_0) = G(s_0) - G(1) + U_{\text{ss}}(s_0): \quad (20)$$

Recall that U_{ss} is the intrinsic dispersion interaction between the two solutes. Values of $W(s_0 = 8A)$ are given in Tab. IV. From system I to VI the total attraction between the solutes decreases almost two orders of magnitude. Interestingly, the curvature correction (I \rightarrow II) lowers W by a large $23.5k_B T$, even though R_0 is small. The reason is that the mean radii

of curvature between the spheres can assume values $\epsilon' \approx 1$, implying that curvature correction is also important for large solutes. A striking effect occurs when vdW contributions are introduced (III–III): the inter solute attraction decreases by approximately $28k_B T$ while the dispersion solute-solute potential $U_{ss}(s_0 = 8A)$ changes by only $0.44k_B T$. Similarly, adding charges of $Z = 5$ (III–V) at the solutes' centers or $Z = 1$ (III–VI) at the solutes' surfaces decreases the total attraction by $1.2k_B T$ and $5k_B T$, respectively. Note that the total attraction decreases even though electrostatic attraction has been added between the solutes. The same trend has been observed recently in explicit water simulations of a similar system of charged hydrophobic nanosolutes.^{29,30}

Now we turn our attention to varying the intersolute distance. The pmfs and solute-solute mean forces $F = -\partial W(s_0)/\partial s_0$ versus a range of s_0 are shown for systems I, II, III, and VI in Fig. 4. System I, with purely repulsive solute-solvent interactions, displays a strong attraction ($W \approx -150k_B T$) at $s_0 = 2A$ which decreases, almost linearly, to zero at a distance $s_0 = 13.5A$ where the system shows a wetting transition. The corresponding force is discontinuous at this critical distance. The steep repulsion at short intersolute distances ($s_0 \approx 1.5A$) stems from the repulsive term of the LJ interaction between the solutes. Note that the intrinsic solute-solute interaction $U_{ss}(s_0)$, also shown in Fig. 4, is almost two orders of magnitude smaller than the hydrophobic attraction. Adding the curvature correction in system II decreases the range and strength of the pmf by approximately 20%, which is significant and unexpected since $R_0 \approx 1$. Adding dispersion attractions in system III decreases the range and strength of the hydrophobic attraction considerably, but it is still much stronger than the inter solute dispersion attraction U_{ss} alone. When surface charges ($Z = 1$) are added in system VI, the range of hydrophobic attraction further decreases but the total attraction increases at short intersolute distances. This is due to the increasing size of the bridging bubble ($r(z = 0)$ increases) as the two solutes approach each other, which decreases the high dielectric screening of the solute-solute electrostatic attraction. This again underlines the importance of coupling electrostatics and dewetting effects, as the electrostatic attraction (or repulsion) may be magnified by more than an order of magnitude when dewetting occurs. For charges with opposite sign this could be interpreted as the stabilization of a salt bridge due to dehydration.⁶⁶ Systems IV and V, not shown in Fig. 4, exhibit the same qualitative behavior as system VI.

4. Comparison of mean forces to previous MD simulations

We continue considering the mean force between two nanosized solutes and compare our theory now to the MD simulations of Dzubilla et al.^{29,30} Their solute model slightly differs from the one used in the previous section: the solute-solvent interaction potential is purely repulsive and is given by $U_i(r) = k_B T (r - R_0)^{-12}$, while the solute-solute interaction is hard-sphere like with a hard sphere radius R_0 . The solutes are neutral or carry opposite charges Q homogeneously distributed over the sphere volume. The simulations were carried out with the SPC/E model of water. In our theory, we fix the Tolman length to $\delta = 0.90\text{\AA}$ as measured by Huang et al.⁴⁹ and the dielectric constant to $\epsilon_1 = 71$ for SPC/E water.⁵⁷ The mean forces are shown in Fig. 5 for neutral spheres of radii $R_0 = 10$ and 12\AA and oppositely charged solutes with radius $R_0 = 10\text{\AA}$ and charge $Q = 2e$ and $5e$ versus the solutes' surface-to-surface distance s_0 . Simulation and theory are in good, almost quantitative agreement, and show that our theory captures the decreasing range of the strongly hydrophobic attraction with decreasing radius and increasing charge due to suppressed dewetting. We emphasize that our theory is basically δ -parameter free for this system of large solutes. Fig. 5 also shows the theoretical mean force for the neutral $R_0 = 12\text{\AA}$ solute using a smaller Tolman length $\delta = 0.75\text{\AA}$. The decrease of the Tolman length increases the depth and range of the solvent-mediated solute-solute attractive mean force by approximately 5%, showing a nonvanishing but only slight influence.

IV. CONCLUSION AND FINAL REMARKS

In summary, we have presented a novel implicit solvent model which couples polar and nonpolar solvation contributions by employing a variational formalism in which the Gibbs free energy of the system is expressed as a functional of the solvent volume exclusion function. Minimization of the free energy leads to a Laplace-Young like equation for the solvent excluded cavity around the solutes, which is extended to describe solvation on mesoscopic and microscopic scales. We have shown that the theory gives a reasonable description of the solvation of microscopic solutes, such as ions and alkanes. Improved accuracy will require further refinement of the curvature dependence of the surface tension $\sigma(\kappa; [v])$ and the definition of the position-dependent dielectric constant $\epsilon(\mathbf{r}; [v])$. Given the physically

reasonable values of the parameters and we found by fitting, we hope that extensions based on physical rationale, e.g. given by complementary microscopic approaches^{15,34,46,67,68} and further empirical corrections, will lead to an accurate ϵ -parameter free implicit solvent description.

We have further demonstrated that on larger scales, where solvent dewetting can play an important role in solvation, our formalism captures the delicate balance between hydrophobic, dispersive and electrostatic forces which has been observed in previous systems.^{20,21,26,27,29,31,32} The dewetting in our model is driven by the interfacial term which favors minimizing the solute-solvent interface. A comment must be made here regarding the sensitivity of dewetting to the particular solvent-solute interactions. As recently argued by Chandler,¹⁷ extended fluid interfaces near phase coexistence are often referred to as 'soft' because they can be deformed with only little or no free-energy change.⁶⁹ Our approach seems to account for this sensitivity since small changes of the constraints in the differential equation (16) for the shape function, given e.g. by the dispersion potential close to the solute surface, can lead to a major deformation or even rupture (wetting transition) of the inter-solute, dewetted region. As we have shown, this can significantly change the pmf for the solutes. Thus we anticipate that slight changes in the geometry of a system, e.g. a slight concave or convex bending of two plate-like solutes,^{20,21} can lead to very different results for the dewetting magnitude and the pmf.

The current illustrations utilized spherical and cylindrical symmetries. More complex molecules, such as proteins, will require solving the full three dimensional problem. Numerical algorithms for the calculation of interface evolution for more complicated geometries are provided by efficient level-set methods or fast marching methods.⁷⁰ We believe that in the full three-dimensional (3D) case, our method will be much more efficient than other microscopic approaches which partly resolve the water structure and are able to describe dewetting effects, e.g. the Lum-Chandler-Weeks theory¹⁵ (LCW) or information theory^{67,68} (IT), as only a two-dimensional surface is sought rather than a 3D density distribution on a fine grid. We remark that LCW and IT do not consider electrostatic interactions and may benefit from our complementary approach.

Acknowledgment

The authors thank Tushar Jain, John Mongan, and Cameron Mura for useful discussions. J.D. and J.M.J.S. acknowledge financial support from a DFG Forschungsstipendium and the PFC-sponsored Center for Theoretical Biological Physics (Grants No. PHY-0216576 and PHY-0225630), respectively. Work in the McCammon group is additionally supported by NIH, HHMI, NBCR, and Accelrys, Inc.

Appendix A : Curvatures in cylindrical coordinates

In our general parametrization for the shape function $r(z)$ we express the radial coordinate by $r = r(l)$ and the axial coordinate by $z = z(l)$, as functions of the parameter l . Depending on the geometry of the considered system, l has to be conveniently chosen, for instance to be the arc length, or $r(l) = l$, or $z(l) = l$. In our illustration the most convenient choice is $z(l) = l$. The principal curvatures are generally given by⁷¹

$$\kappa_1(r; z) = \frac{z'}{r \sqrt{z'^2 + r'^2}}; \quad \kappa_2(r; z) = \frac{z'' r' - z' r''}{(z'^2 + r'^2)^{3/2}}; \quad (21)$$

where the primes indicate the partial derivative with respect to l . Additionally, the unit normal vector reads

$$\mathbf{n}(r; z) = \frac{1}{\sqrt{z'^2 + r'^2}} \begin{pmatrix} z' \\ r' \end{pmatrix} \quad (22)$$

The differential equation (16) is then solved by a forward relaxation scheme in time t

$$\frac{\partial}{\partial t} \begin{pmatrix} r(t+\Delta t) \\ z(t+\Delta t) \end{pmatrix} \mathbf{A} = \begin{pmatrix} r(t) \\ z(t) \end{pmatrix} \mathbf{A} - \Delta t \mathbf{n}(r; z) d\epsilon(r; z); \quad (23)$$

where the steady-state solution $\epsilon(r; z) = \epsilon(t = 0)$ is the solution of $d\epsilon(r; z) = 0$ we are looking for. In the numerical calculations we use a grid of 500 bins and an integration time step of $\Delta t = 0.001$. The first and second derivatives are approximated using a symmetric two and three-step finite difference equation, respectively. Convergence is usually reached after 10 time steps. The result is observed to be independent of the initial choice of $r(z)$ at $t = 0$.

Appendix B : Numerical solution of the PB equation

Since we neglect mobile ions in our work, the PB equation reduces to Poisson's equation. It is solved on a two dimensional grid in cylindrical coordinates r and z with a finite difference method. The gradient and Laplacian are given then by $\nabla = (\partial_r; \partial_z)$ and $\nabla^2 = \partial_r^2 + \partial_z^2$, respectively. The first and second derivatives are approximated using symmetric two or three-step finite-difference equations. An explicit, forward time relaxation scheme is used to find the solution of Poisson's equation:

$$\psi(t + \Delta t; \mathbf{r}) = \psi(t; \mathbf{r}) - \Delta t \nabla^2 \psi(t; \mathbf{r}) \quad (24)$$

In most cases we use a lattice spacing of $\Delta r = \Delta z = 0.4 \text{ \AA}$ on a $n_r \times n_z = 100 \times 200$ grid, and an integration time step $\Delta t = 0.05$. Convergence takes approximately 10^5 time steps. For the charged particles which are buried in the nanosolutes we use homogeneously charged spheres with a radius of 2 \AA . Instead of a sharp transition for the dielectric boundary (12), we use a smoothing function for reasons of numerical stability:

$$\epsilon(\mathbf{r}) = \frac{1}{\exp(-d(\mathbf{r})/\lambda) + 1} + \epsilon_v \quad (25)$$

where the absolute value of the length $d(\mathbf{r})$ is given by the nearest distance to the boundary of the volume exclusion function $v(\mathbf{r})$. d is defined to be positive when $\mathbf{r} \in V$ and negative elsewhere. The inverse length λ defines the width of the boundary region and in the limit

$\lambda \rightarrow 0$ we recover the sharp transition (12). We choose a value $\lambda = 3 \text{ \AA}$ for which the solution of Poisson's equation becomes basically independent of the choice of λ . An example for the dielectric boundary is shown in Fig. 6 for two partly dewetted nanosolutes of radius $R_0 = 15 \text{ \AA}$ at a distance $s_0 = 7 \text{ \AA}$ carrying a charge $Q = 5e$ (system V in sec. III.C).

In order to obtain the optimal shape function $v_{\text{min}}(\mathbf{r})$ the shape equation (16) has to be solved simultaneously with Poisson's equation when the solutes are charged. In practice, we first solve (16) without any electrostatic contributions. In the second step, we solve Poisson's equation with the dielectric boundary (25) given by the volume exclusion function of the former solution. The result for the electric energy density is then plugged back in the shape equation in the third step. The last two steps are repeated until the solution for $v_{\text{min}}(\mathbf{r})$ is fully converged. Since the results for $r(z)$ excluding and including electrostatics are quite similar for our systems, full convergence takes usually only 6 to 7 repetitions of

the described iteration steps.

e-mail address: jdzubiella@ucsd.edu

- ¹ B. Roux and T. Simonson, *Biophys. Chem.* **78**, 1 (1999).
- ² F. M. Richards, *Annu. Rev. Biophys. Bioeng.* **6**, 151 (1977).
- ³ E. Gallicchio, M. M. Kubo, and R. M. Levy, *J. Phys. Chem. B* **104**, 6271 (2000).
- ⁴ E. Gallicchio, L. Y. Zhang, and R. M. Levy, *J. Comput. Chem.* **23**, 517 (2002).
- ⁵ M. Zacharias, *J. Chem. Phys. A* **107**, 3000 (2003).
- ⁶ Y. Su and E. Gallicchio, *Biophys. Chem.* **109**, 251 (2004).
- ⁷ R. M. Levy, L. Y. Zhang, E. Gallicchio, and A. K. Felts, *J. Am. Chem. Soc.* **125**, 9523 (2003).
- ⁸ D. Bashford and D. A. Case, *Ann. Rev. Phys. Chem.* **51**, 129 (2000).
- ⁹ K. A. Sharp and B. Honig, *J. Phys. Chem.* **94**, 7684 (1990).
- ¹⁰ D. Baker, *Curr. Opin. Struct. Bio* **15**, 137 (2005).
- ¹¹ M. Nina, D. Beglov, and B. Roux, *J. Phys. Chem. B* **101**, 5239 (1997).
- ¹² D. M. Huang and D. Chandler, *J. Phys. Chem. B* **106**, 2047 (2002).
- ¹³ H. S. Ashbaugh, E. W. Kaler, and M. E. Paulaitis, *Biophys. J.* **75**, 755 (1998).
- ¹⁴ F. H. Stillinger, *J. Solution Chem.* **2**, 141 (1973).
- ¹⁵ K. Lum, D. Chandler, and J. D. Weeks, *J. Phys. Chem. B* **103**, 4570 (1999).
- ¹⁶ G. Hummer, L. R. Pratt, and A. E. Garcia, *J. Chem. Phys.* **107**, 9275 (1997).
- ¹⁷ D. Chandler, *Nature* **437**, 640 (2005).
- ¹⁸ A. Wallquist and B. J. Berne, *J. Phys. Chem.* **99**, 2893 (1995).
- ¹⁹ X. Huang, C. J. Margulis, and B. J. Berne, *PNAS* **100**, 11953 (2003).
- ²⁰ X. Huang, R. Zhou, and B. J. Berne, *J. Phys. Chem. B* **109**, 3546 (2005).
- ²¹ N. Choudhury and B. M. Pettitt, *J. Am. Chem. Soc.* **127**, 3556 (2005).
- ²² G. Hummer, J. C. Rasaiah, and J. P. Nowortya, *Nature* **414**, 188 (2001).
- ²³ R. Allen, S. Melchionna, and J. P. Hansen, *Phys. Rev. Lett.* **89**, 175502 (2002).
- ²⁴ O. Beckstein, P. C. Biggin, and M. S. P. Sansom, *J. Phys. Chem.* **105**, 12902 (2001).
- ²⁵ A. Anishkin and S. Sukharev, *Biophys. J.* **86**, 2883 (2004).
- ²⁶ J. Dzubiella and J. P. Hansen, *J. Chem. Phys.* **120**, 5001 (2004).
- ²⁷ S. Vaitheeswaran, J. C. Rasaiah, and G. Hummer, *J. Chem. Phys.* **121**, 7955 (2004).

- ²⁸ J. D. Zubiella and J.-P. Hansen, *J. Chem. Phys.* **122**, 234706 (2005).
- ²⁹ J. D. Zubiella and J.-P. Hansen, *J. Chem. Phys.* **119**, 12049 (2003).
- ³⁰ J. D. Zubiella and J.-P. Hansen, *J. Chem. Phys.* **121**, 5514 (2004).
- ³¹ R. Zhou, X. Huang, C. Margulis, and B. J. Beme, *Science* **305**, 1605 (2004).
- ³² P. Liu, X. Huang, R. Zhou, and B. J. Beme, *Nature* **437**, 159 (2005).
- ³³ J. L. Parker, P. M. Claesson, and P. Attard, *J. Phys. Chem.* **98**, 8468 (1994).
- ³⁴ D. Beglov and B. Roux, *J. Chem. Phys.* **104**, 8678 (1996).
- ³⁵ P. Kralchevsky and K. Nagayama, *Particles at Fluid Interfaces and Membranes* (Elsevier, 2001, Amsterdam).
- ³⁶ W. Helfrich, *Z. Naturforsch. C* **28**, 693 (1973).
- ³⁷ O.-Y. Zhong-can and W. Helfrich, *Phys. Rev. A* **39**, 5280 (1989).
- ³⁸ T. Bieker and S. Dietrich, *Physica A* **252**, 85 (1998).
- ³⁹ T. Chou, *Phys. Rev. Lett.* **87**, 106101 (2001).
- ⁴⁰ R. Allen, S. Melchionna, and J.-P. Hansen, *J. Chem. Phys.* **119**, 3905 (2003).
- ⁴¹ P. Attard, *Langmuir* **16**, 4455 (2000).
- ⁴² Y.-K. Cheng and P. J. Rossky, *Nature* **392**, 696 (1998).
- ⁴³ M. Gerstein and C. Chothia, *Proc. Natl. Acad. Sci. USA* **93**, 10167 (1996).
- ⁴⁴ K. K. S. Lau, J. Bico, K. B. K. Teo, M. Chhowalla, G. A. J. Amaratunga, W. I. Milne, G. H. McKinley, and K. K. Gleason, *Nano Letters* **3**, 1701 (2003).
- ⁴⁵ J. D. Zubiella, J. M. J. Swanson, and J. A. McCammon (2005), to be published.
- ⁴⁶ D. G. Triezenberg and R. Zwanzig, *Phys. Rev. Lett.* **28**, 1183 (1972).
- ⁴⁷ J. D. Jackson, *Classical Electrodynamics* (Wiley, New York, 1999), 3rd edn.
- ⁴⁸ M. K. Gilson, M. E. Davis, B. A. Luty, and J. A. McCammon, *J. Phys. Chem.* **97**, 3591 (1993).
- ⁴⁹ D. M. Huang, P. L. Geissler, and D. Chandler, *J. Phys. Chem. B* **105**, 6704 (2001).
- ⁵⁰ The principal curvatures are formally given by the eigenvectors of the Hessian (or shape operator) of v, \hat{S} , which can be expressed by the vector gradient of the unit normal vector field $\mathbf{n}(\mathbf{r})$ of the surface, $\hat{S} = \mathbf{r} \cdot \mathbf{n}(\mathbf{r}) = \mathbf{r} \cdot \frac{\mathbf{r} \times \nabla(\mathbf{r})}{|\mathbf{r} \times \nabla(\mathbf{r})|}$.
- ⁵¹ J. R. Henderson, *Fundamentals of Inhomogeneous Fluids* (Dekker, New York, 1992), edited by D. Henderson.
- ⁵² M. C. Stewart and R. Evans, *Phys. Rev. E* **71**, 011602 (2005).
- ⁵³ H. Reiss, *Adv. Chem. Phys.* **9**, 1 (1965).

- ⁵⁴ R. C. Tolman, *J. Chem. Phys.* 17, 333 (1949).
- ⁵⁵ A. Nicholls, K. A. Sharp, and B. Honig, *Proteins* 11, 281 (1991).
- ⁵⁶ H. Luo and C. Tucker, *J. Phys. Chem.* 100, 11165 (1996).
- ⁵⁷ H. J. C. Berendsen, J. R. Grigera, and T. P. Straatsma, *J. Phys. Chem.* 91, 6269 (1987).
- ⁵⁸ S. R. Manjari and H. J. Kim, *J. Chem. Phys.* 123, 014504 (2005).
- ⁵⁹ G. Hummer, L. R. Pratt, and A. E. Garcia, *J. Phys. Chem.* 100, 1206 (1996).
- ⁶⁰ D. Paschek, *J. Chem. Phys.* 120, 6674 (2004).
- ⁶¹ J. Alejandre, D. J. Tildesley, and G. A. Chapela, *J. Chem. Phys.* 102, 4574 (1995).
- ⁶² M. L. Connolly, *J. Mol. Graphics* 11, 139 (1993).
- ⁶³ The solute-solute LJ parameters have been calculated from the solute-water LJ parameters employing the usual combining rules. Note that the rules used by Ashbaugh et al.,¹³ are different to those of Hummer et al.⁵⁹ and Paschek⁶⁰.
- ⁶⁴ D. van der Spoel, P. J. van Maaren, and H. J. C. Berendsen, *J. Chem. Phys.* 108, 10220 (1998).
- ⁶⁵ W. Jorgensen, J. D. Madura, and C. J. Swenson, *J. Am. Chem. Soc.* 106, 6638 (1984).
- ⁶⁶ A. Fernandez, *Nature Biotech.* 22, 1081 (2004).
- ⁶⁷ G. Hummer, S. Garde, A. E. Garcia, A. Phorille, and L. R. Pratt, *Proc. Natl. Acad. Sci. USA* 93, 8951 (1996).
- ⁶⁸ S. Garde, G. Hummer, A. E. Garcia, M. E. Paulaitis, and L. R. Pratt, *Phys. Rev. Lett.* 77, 4966 (1996).
- ⁶⁹ S. A. Safran, *Statistical Thermodynamics of Surfaces, Interfaces and Membranes* (Addison-Wesley, Reading, 1994), ch. 1-3.
- ⁷⁰ J. A. Sethian, *Level Set methods and Fast Marching Methods: Evolving Interfaces in Geometry, Fluid Mechanics, Computer Vision, and Materials Science* (Cambridge University Press, Cambridge, 1999).
- ⁷¹ T. Frankel, *The Geometry of Physics* (Cambridge University Press, Cambridge, 1997).

Solute	ϵ (kJ=m ol)	σ Å	G_{sim} (kJ=m ol)	r_{bf} Å	R_{min} Å
SPC	0.65	3.17	{	{	{
SPC /E	0.65	3.17	{	{	{
ref ⁵⁹					
Na ⁰	0.2005	2.85	9.2 (1)	0.79	2.32
K ⁰	0.0061	4.52	23.7 (5)	0.76	2.83
Ca ⁰	0.6380	3.17	10.2 (3)	0.85	2.80
F ⁰	0.5538	3.05	9.7 (2)	0.85	2.68
Cl ⁰	0.5380	3.75	21 (3)	0.80	3.30
Br ⁰	0.4945	3.83	24 (3)	0.77	3.35
ref ⁶⁰					
Ne	0.3156	3.10	11.41 (0.05)	0.84	2.61
Ar	0.8176	3.29	8.68 (0.08)	0.90	2.96
Kr	0.9518	3.42	8.12 (0.1)	0.91	3.10
Xe	1.0710	3.57	7.65 (0.15)	0.92	3.27
ref ¹³					
Me	0.8941	3.44	10.96 (0.46)	0.85	3.11
ethane	{	{	10.75 (0.50)	0.87	{
CH ₃	0.7503	3.46	{	{	{
propane	{	{	13.81 (0.54)	0.94	{
butane	{	{	14.69 (0.54)	0.96	{
CH ₂	0.5665	3.52	{	{	{
CH ₃	0.6900	3.52	{	{	{

TABLE I: Solute-water LJ parameters and solvation free energy G_{sim} for neutral Lennard-Jones spheres from the SPC water simulations performed by Hummer et al.⁵⁹ and Paschek.⁶⁰ r_{bf} is the Tolman length best fit to G_{sim} (rounded to two digits after the decimal point). R_{min} is the resulting optimal radius excluded of solvent. Also shown are the values for the simple alkanes methane (Me), ethane, propane, and butane from the study of Ashbaugh et al.¹³ Simulation errors are given in parentheses.

Atom	$G_{\text{sim}} = (\text{kJ mol}^{-1})$	$r_{\text{bf}} = \text{\AA}$	$R_{\text{min}} = \text{\AA}$
Ne	11.65 (0.05)	0.88	2.60
Ar	8.83 (0.08)	0.96	2.94
Kr	8.20 (0.1)	0.98	3.09
Xe	7.58 (0.15)	1.00	3.25

TABLE II: Solvation free energies for neutral Lennard-Jones spheres in SPC/E water from the simulations of Paschek.⁶⁰ r_{bf} and R_{min} are defined as in Tab. I.

Ion	q	$\frac{G_{\text{sim}}}{\text{kJ mol}^{-1}}$	$\frac{G}{\text{kJ mol}^{-1}}$	$\frac{G}{\text{kJ mol}^{-1}}$	$R_{\text{min}} = \text{\AA}$
Na^+	1	-398	-334	-394	1.83
K^+	1	-271	-246	-282	2.35
Ca^{2+}	2	-1306	-1181	-1364	2.09
F	-1	-580	-274	-630	2.25
Cl	-1	-371	-198	-342	2.97
Br	-1	-358	-192	-328	3.02

TABLE III: Solvation free energies for charged LJ spheres in SPC water from the simulations of Hummer et al.⁵⁹ compared to the theoretical result G . For r_{bf} we use the best fits r_{bf} to the solvation of neutral spheres as shown in Tab. I. G is the result when the dielectric boundary shift is applied, see text.

System	ϵA	vdW attraction	Z	$W(s_0) = k_B T$	dewetted
I	0.00	no	0	-57.6	yes
II	0.75	no	0	-34.1	yes
III	0.75	yes	0	-6.3	yes
IV	0.75	yes	4	-9.2	yes
V	0.75	yes	5	-5.1	no
VI	0.75	yes	1 (oc)	-1.3	no

TABLE IV : Studied systems for two alkane-assembled spherical solutes. $W(s_0)$ is the inter-solute pm f. If $r(z=0) \neq 0$ the system is 'dewetted'. In system VI the solutes' charge is located on-center (oc) at the solute surface.

FIG. 1: The particular solvation energy contributions $G_i(R)$ with $i = p, \text{int}, \text{ne}$ in Eq. (18) for one LJ sphere with Na^0 parameters given in Tab. I. The pressure term G_{pr} (thin solid line) with $P = 1 \text{ atm}$ is basically zero on this scale. The interfacial term $G_{\text{int}}(R)$ (dotted line) with $\gamma = 65 \text{ mJ/m}^2$ increases with radius R . The LJ term $G_{\text{ne}}(R)$ is given by the dashed line. The sum of the three contribution gives the total $G(R)$ (solid line) with a minimum at $R_{\text{min}} = 2.32 \text{ \AA}$ for the uncharged sodium Na^0 . The inset shows the electrostatic contribution $G_{\text{es}}(R)$ (dot-dashed line) and the total $G(R)$ for the charged Na^+ with a minimum at $R_{\text{min}} = 1.83 \text{ \AA}$. The best-fit Tolman length is $\delta_f = 0.79 \text{ \AA}$.

FIG. 2: Mean $H(z)$ and Gaussian $K(z)$ curvature and shape function $r(z)$ (solid lines) for ethane. The canonical SAS (dashed line) from rolling a probe sphere with radius $r_p = 1.4 \text{ \AA}$ over the vdW surface (shaded region) is also shown. The vdW surface is defined by the solute-solute LJ-radius $\sigma_{ss} = 2 = 1.73 \text{ \AA}$.⁶³

FIG. 3: Mean $H(z)$ and Gaussian $K(z)$ curvatures and shape function $r(z)$ for two alkane-assembled solutes of radius $R_0 = 15 \text{ \AA}$ (shaded region) at a distance $s_0 = 8 \text{ \AA}$ for systems I-VI. The position of the charges $Z = -1$ in VI are indicated by arrows. Curvatures are not shown for the ‘wet’ systems V and VI.

FIG. 4: Top frame: theoretical pmfs for the systems I-III, and VI versus the solute distance s_0 . Bottom frame: corresponding mean forces.

FIG. 5: Mean force $\langle F_A \rangle$ between two nanosized solutes versus surface-to-surface distance s_0 . The symbols denote the MD simulation results from Dziubiella et al.^{29,30} for neutral spheres with radius $R_0 = 12\text{\AA}$ (circles) and $R_0 = 10\text{\AA}$ (squares), and oppositely charged spheres with radius $R_0 = 10\text{\AA}$ and charge $Q = 2e$ (diamonds) and $Q = 5e$ (triangles). The corresponding theoretical results using $\epsilon = 0.9$ are shown by solid lines; the range of the strong hydrophobic attraction decreases with decreasing radius and increasing charge. Dotted lines through the symbols are guides for the eye. The dashed line is the theory for $R_0 = 12\text{\AA}$ and $\epsilon = 0.75$.

FIG. 6: Distribution of the dielectric constant in space for two nanosolutes with $R_0 = 15\text{\AA}$ at a distance $s_0 = 7\text{\AA}$ carrying a charge $Q = 5e$ (system V). The region between the spheres is dewetted. The distribution is scaled by $\epsilon_1 = 78$.

Figure 1

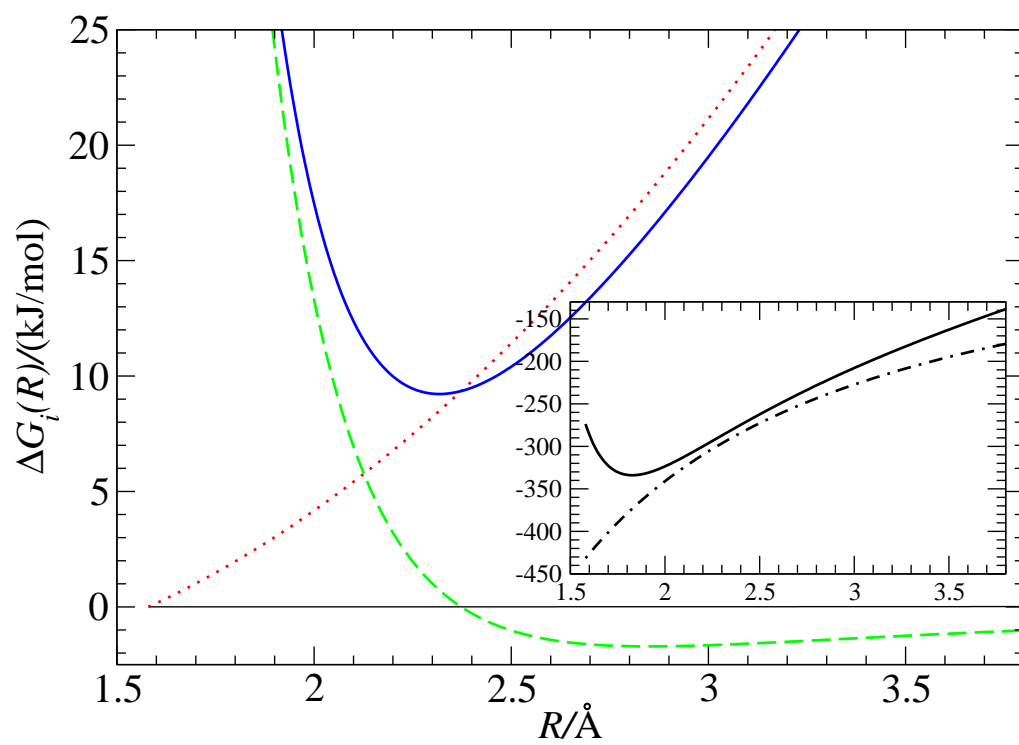


Figure 2

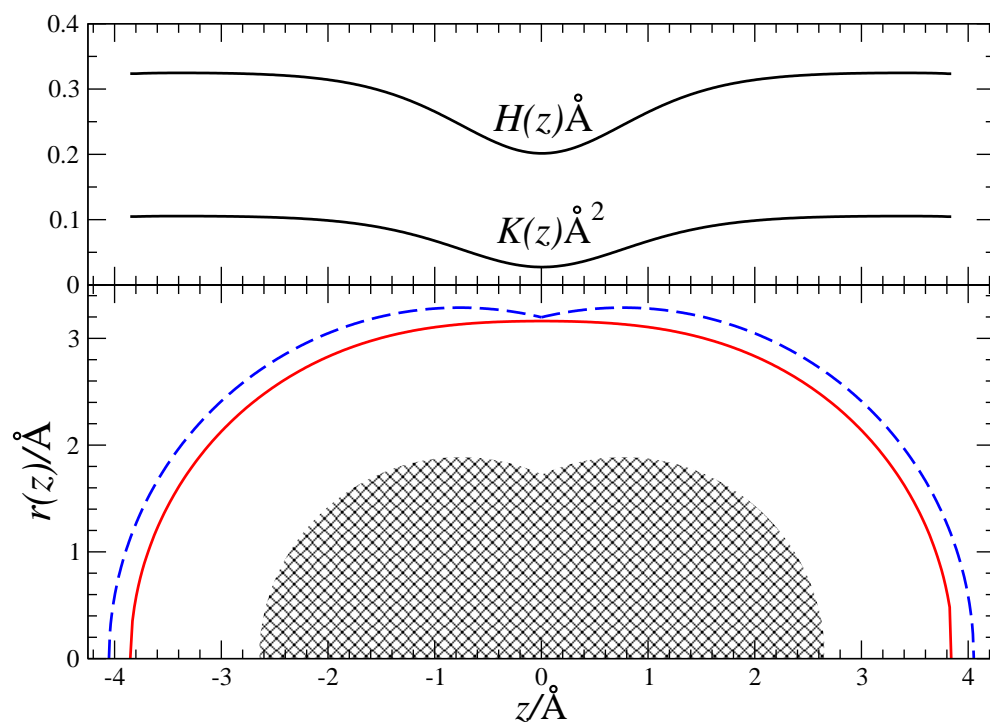


Figure 3

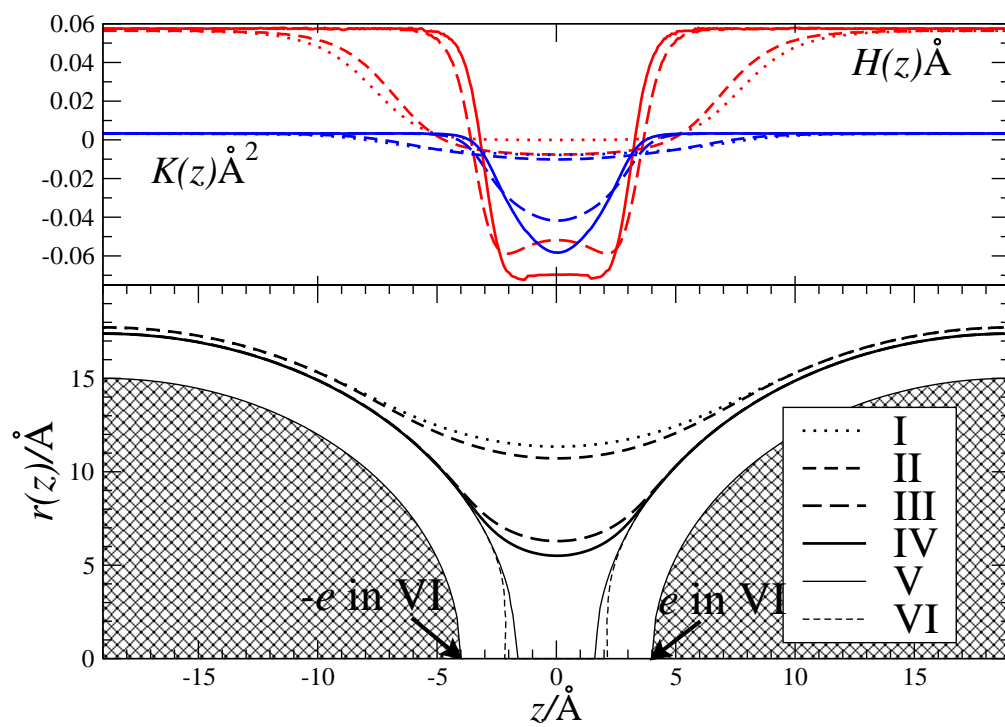


Figure 4

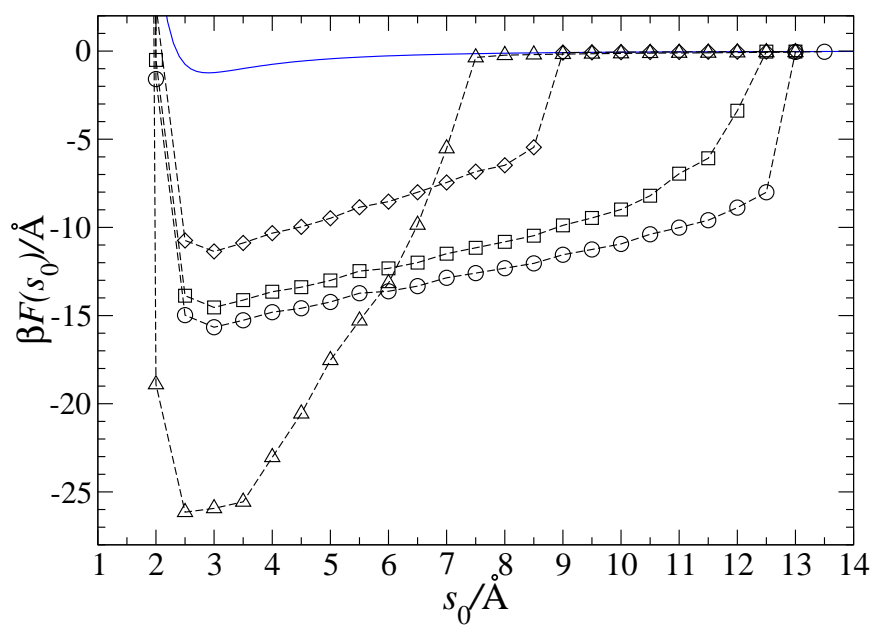
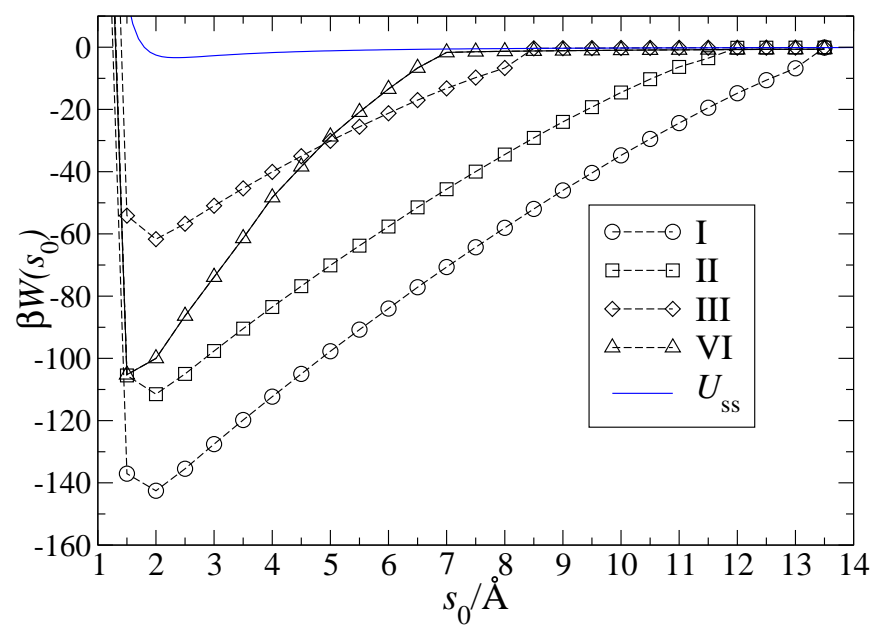


Figure 5

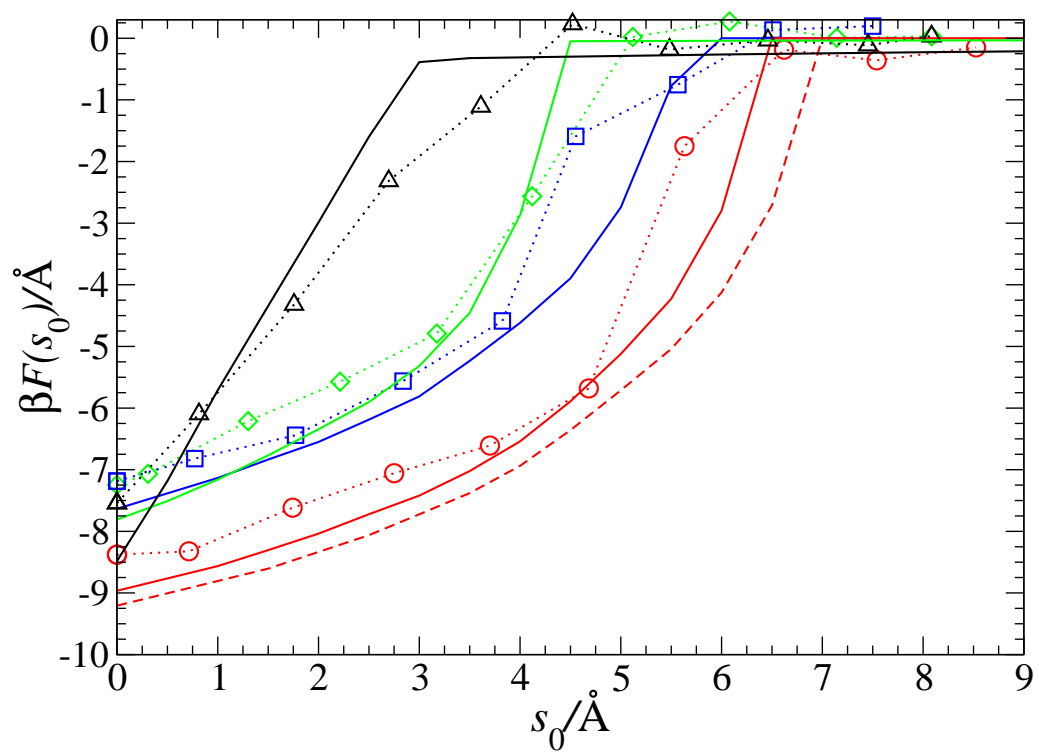


Figure 6

